Journal of Engineering Science and Technology
Vol. 18, No. 3 (2023) 1791 - 1804

MECHANICAL DESIGN AND OPTIMISATION OF LUMBAR DISC PROSTHESIS MODEL

K. Y. SARA LEE[1], W. J. TAN[1], S. RAMESH[2,3], ABDULKAREEM SH. MAHDI AL-OBAIDI[4]

[1]Center of Systematic Innovation Research, Department of Mechanical Engineering, Faculty of Engineering and Technology, Tunku Abdul Rahman University of Management and Technology, 53300 Kuala Lumpur, Malaysia
[2]Center of Advanced Manufacturing and Material Processing, Department of Mechanical Engineering, Faculty of Engineering, University of Malaya, 50603 Kuala Lumpur, Malaysia
[3]Universiti Tenaga Nasional, Putrajaya Campus, Jalan IKRAM-UNITEN, 43000 Kajang, Selangor, Malaysia
[4]School of Engineering, Faculty of Innovation and Technology, Taylor's University, Taylor's Lakeside Campus, Subang Jaya, Selangor DE, Malaysia
*Corresponding Author: leeky@tarc.edu.my

Abstract

The effect of dimensions on the safety factor, allowable stress, and deformation of the lumbar disc prosthesis model at L4-L5 was investigated. The process involved geometry design, meshing, enhancement in element quality, and setting of boundary conditions using SolidWorks and ANSYS software. The range of motion (ROM) of flexion and extension were measured using SolidWorks Limit Angle. Additionally, the direct optimisation method was utilised to determine the optimal input parameters and dimensions for the lumbar disc prosthesis model. The results showed a wide ROM for flexion and extension of the model, which ranged from 20° to -11° when Polyetheretherketone (PEEK) was selected as the biomaterial. The distribution of stress and deformation of the model during neutral, flexion and extension are presented. An overview of the optimised dimensions that satisfied the requirements for safety factor (more than 2), allowable stress (70.2 MPa) and deformation (62.11 μm) for the model are deliberated. Three optimised input diameters and heights of 10.2 mm x 0.279 mm, 11.4 mm × 1.591 mm and 13 mm x 1.810 mm were proposed for the lumbar disc prosthesis model. The safety factor, maximum stress and deformation of the proposed dimensions ranged from 2 to 2.11, 52.32 to 55.12 MPa and 30.14 to 37.98 μm, respectively.

Keywords: Deformation, Extension, Flexion, Lumbar disc prosthesis, Optimisation, Stress.

1. Introduction

Degenerative Disc Disease (DDD) often results in persistent and incapacitating pain in the lower back. One treatment option for DDD is total disc replacement surgery, which aims to restore functional motion to the affected area of the spine. During the procedure, the damaged disc is removed and replaced with an artificial disc, known as a lumbar disc prosthesis [1]. The fundamental unit of the spine, known as the Functional Spinal Unit (FSU), is composed of two contiguous vertebrae, intervertebral disc that lies between them, and the ligaments and joints that interconnect them both structurally and functionally. The lumbar disc, located between the lumbar vertebrae in the lower back, is a crucial component of the FSU [2].

A fundamental function of disc prostheses is to enable the relative movement of vertebral bodies through slippage between the surfaces of their respective components. Design concepts for lumbar disc can be classified into two types: constrained and unconstrained designs [3]. Constrained designs are characterized by a fixed location of the instantaneous axis of rotation of the intervertebral joint, determined by the prosthesis kinematics. On the other hand, unconstrained designs rely on the combined action of the prosthesis, ligaments, facet joints, and muscles to determine this axis. Constrained designs typically employ a ball-and-socket joint, where the axis of rotation passes through the centre of the spherical surfaces forming the joint. Examples of constrained designs include the Maverick and ProDisc prostheses [4-6]. An example of an unconstrained design is the Charite, which operates by means of a mobile core articulating with two opposing bearing surfaces anchored to each of the vertebral bodies [7, 8].

In general, the lumbar spine consists of five lumbar discs and is located at L1-L2, L2-L3, L3-L4, L4-L5, and L5-S1, respectively. Specifically, L4-L5 plays an important role in supporting the upper body, which are the two lowest vertebrae of the lumbar spine [9, 10]. Besides, L4-L5 segment has the highest incidence of degeneration [11]. Throughout the years, investigations have been widely carried out on lumbar discs located at L4-L5 using finite element analysis (FEA). Various finite element modeling software was used in the analysis of lumbar disc model such as SolidWorks[12], ABAQUS [11, 13, 14], Autodesk Fusion 360 [15] and ANSYS [12, 16], where mesh properties, boundary conditions and material properties were set. For example, mechanical responses of a shape memory polymers intervertebral disc model positioned at L4-L5 were determined using analytical methods combined with numerical analysis, FEA with ABAQUS [14]. FEA enables the analysis of lumbar spine deformation, stress distribution, and strain, thereby obviating the requirement for physical specimens. This method employs simulations of manipulations such as flexion, extension, and torsion to obtain information about these parameters at any point on the lumbar spine. While FEA cannot replace conventional biomechanical investigations, it serves as an indispensable and potent supplement to in vitro experiments or biomedical applications [12, 17, 18].

Rotational range of motion (ROM) such as flexion, extension, lateral bending, and axial torsion were commonly assessed to describe the biomechanical behavior of the lumbar disc prosthesis. Besides, FEA on stress and deformation in various scenarios were often investigated in various studies [19-22]. According to literature, typical ROM for L4–L5 reported an average flexion of 13°, extension of

-3°, and lateral bending of 3° [23]. In a study [1], implantation of Maverick devices at L4-L5 in cadaveric spinal segments resulted in a 5.4° increase in flexion and extension, from 10.9° to 16.3°. Alternatively, 100 CHARITE´ demonstrated a higher flexion-extension of 9.6° and lateral bending of 5.4° at L4-L5 [24]. For ProDisc-L implant, the ROM for flexion and extension was recorded to range from 4.1 to -7.6° [1].

The spine is subjected to load resulting from a combination of weight, muscle activity, and ligament pull. Posture has a significant impact on the loading of the spine, with the muscles causing more depression in a standing position. Typically, the center of gravity is located in front of the lumbar spine. The range of loads for daily activities with normal motion ranges from 250 N to 950 N, including sitting upright with or without support, standing and coughing [25]. These loads were applied to simulate the flexion-extension range of motion of a lumbar disc model. For instance, a loading force of 300 N was applied to the lumbar disc to simulate stress distribution while sitting and side-lying [12]. On the other hand, a 400 N load was applied to a disc prosthesis to simulate the flexion-extension range of motion under a physiological compression load [3]. Similarly, a 400 N force was loaded onto the lumbar disc to simulate physical standing posture's stress distribution and range of motion in daily life [6]. A higher load of 500 N was also been used in another study on lumbar disc, with a subject weighing 68 kg to simulate various postures [26].

Recent research and innovation in the field of lumbar surgery have shown promising results. However, there is still a significant gap in knowledge on identifying the optimal biomaterials and design parameters for lumbar disc prostheses. Various engineering materials have been widely studied for a variety of biomedical applications including coatings, ceramics, polymers and metals [27-29]. However, the most commonly used biomaterials for lumbar disc replacements are Titanium (Ti), Cobalt Chromium (CoCr) alloy, Ultrahigh Molecular Weight Polyethylene (UHMWPE), Polyurethane Polycarbonate Elastomer (PU-PC), silicone and diamond-like carbon coatings [30]. Some of the popular implants that used Co-Cr-UHMWPE as the biomaterials are CHARITE´, Activ-L, and Mobidisc, and ProDisc-L. However, CHARITE´, Activ-L, and Mobidisc have experienced damage on polyethylene surface, innate periprosthetic inflammation, and polyethylene wear debris.

Besides, ProDisc-L devices also showed metal wear debris and endplate impingement [30, 31]. On the other hand, metallic debris was also detected on Maverick and Kineflex devices that used CoCr-CoCr [31, 32]. In view of the complications triggered by other biomaterials, Polyetheretherketone (PEEK) has gained attention as a potential biomaterial for spinal implant applications and lumbar disc replacement. PEEK is one of the nontoxic high-performance thermoplastics that were extensively employed in various medical applications [33]. PEEK exhibits excellent biocompatibility and non-toxic to human body, which could prevent the damage to human tissues or cells.

One of the advantages of PEEK as implant material is its low elastic modulus, which is similar to human trabecular bone. Typically, the elastic modulus of a PEEK is 3–4 GPa, which is significantly lower than Ti (102–110 GPa). The low elastic modulus of PEEK that is closer to human trabecular bone (1 GPa) could minimise stress shielding, reduce the risk of bone resorption and implant loosening [34]. Given

the potential benefits of using PEEK as implant material for lumbar disc replacement, it is crucial to investigate the mechanical behaviour, including stress, deformation, flexion and extension motion of PEEK-based lumbar disc prosthesis.

The objective of this study was to study the stress, deformation, flexion, and extension motion of lumbar disc prosthesis model at L4-L5 using PEEK. Besides, direct optimisation was employed to identify the optimum parameters for the model using FEA with the combinations of SolidWorks and ANSYS.

2. Methodology

2.1. Geometry design and parameters

The design of lumbar disc prosthesis model focused on the L4-L5 location. SolidWorks software was used for geometry design, and ANSYS software was used for the simulation, analysis, and optimisation. The ROM of flexion and extension of the model were then measured using SolidWorks Limit Angle. Figure 1 shows the general view of the model, which consists of upper and lower parts. This design was inspired by the ball and socket human hip joint and synovial joint [35]. The upper part consists of the upper endplate with fixation and ball (core), and the lower part consists of the lower endplate with fixation and socket. Figures 2(a) and (b) show the multiple views of the upper and lower parts of the model, respectively. The width and length of the model were set to be 24 and 33 mm respectively, according to the typical range of natural lumbar vertebrae and disc [36].

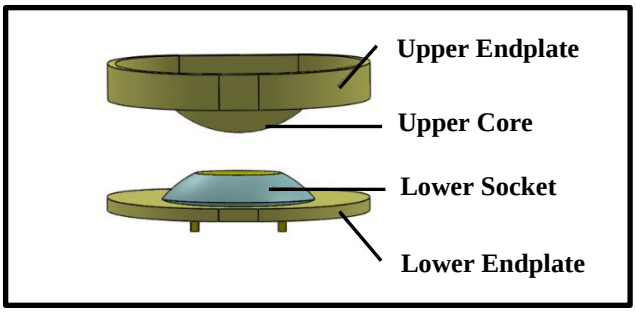

Fig. 1. General view of lumbar disc prosthesis model design.

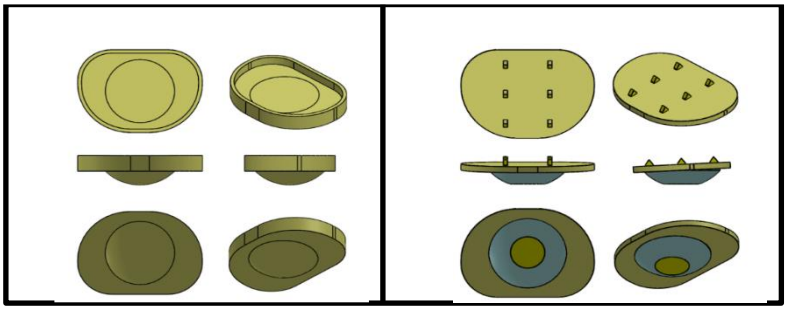

(a) Upper part. **(b) Lower part.**

Fig. 2. Multiple views of lumbar disc prosthesis model design (a) Upper part and (b) Lower part.

2.2. Meshing properties

The geometry of the design was meshed with an average surface area of $3.09 \times 10^{-5}\, m^2$ and average element size of $2.17 \times 10^{-3}\, m$. Table 1 shows the initial and final meshing parameters. The final meshed design was improved in average element quality, with a maximum element quality of 0.99971. Besides, the number of nodes and elements had increased to 488710 and 311088, respectively. The standard deviation was reduced to 0.126, which contributed to higher accuracy and consistency.

Table 1. Meshing parameters for initial and final meshing.

Meshing Parameters	Initial Meshing	Final Meshing
Nodes	10813	488710
Elements	5786	311088
Average element quality	0.674	0.744
Standard deviation of element quality	0.154	0.126

With the aid of element quality chart (Fig. 3), the location of low element quality was identified and meshed into finer elements using face sizing, face meshing and refinement methods etc. The final meshed design for the model is illustrated in Fig. 4. In addition, convergence test was also conducted to achieve an allowable change of 5% with h-adaptive refinement loop for better accuracy.

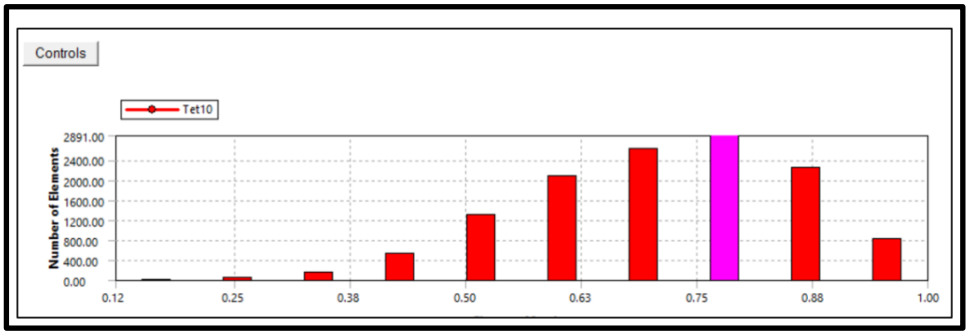

Fig. 3. Element quality chart.

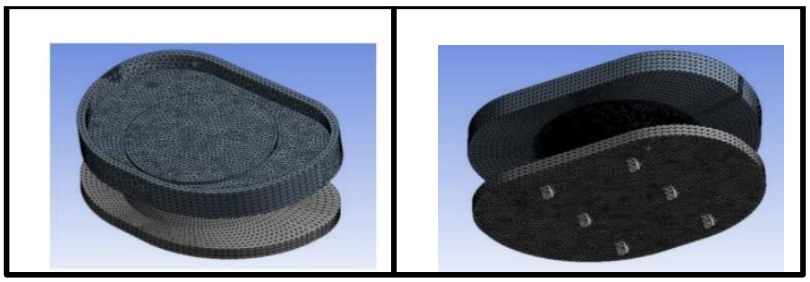

(a) Isometric view. **(b) Side view.**

Fig. 4. Final meshed design of lumbar disc prosthesis model (a) Isometric view and (b) Side view.

2.3. Boundary condition

The design was based for females aged from 35 to 45 years old, body weight from 40 to 50 kg and height from 148 to 160 cm. As the average mass of the lower trunk of the human body is 22 kg, a load of 216 N was applied to the prosthesis. PEEK was used as the material for the lumbar disc prosthesis model, with a Young's Modulus of 3.95 GPa and tensile strength of 110 MPa.

2.4. Direct optimisation

Direct optimisation method was employed to select the best input parameters through an iterative process, with the objective of maximising or minimising the output parameters. The input parameters for this design are diameter (10-22 mm) and height (0.25-2 mm) as in Fig. 5. The optimisation goals (output parameters) were set to achieve a maximum value for the minimum safety factor, a minimum value for the deformation and Von Mises stresses. The simulation was set to generate 30 samples to obtain the optimum diameter and height for model by considering the given load and geometry design.

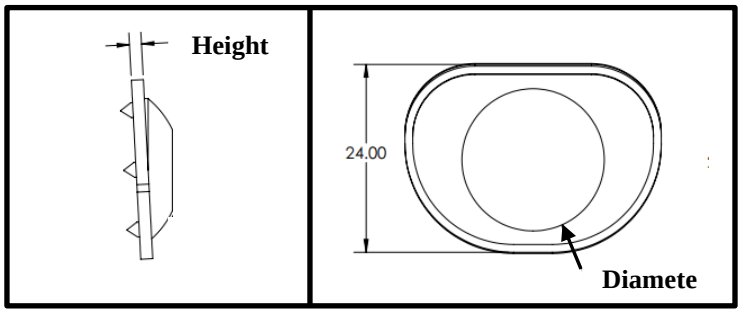

(a) Side view. **(b) Top view.**

Fig. 5. Height and diameter of lumbar disc prosthesis model (a) Side view and (b) Top view.

3. Results and Discussion

The distribution of stress and deformation with the applied load of 216 N was demonstrated. The range of motion, including flexion and extension motions, was measured and compared with other existing designs. Additionally, stress and deformation were generated during flexion and extension motions. As the typical load range is between 200 and 950 N for daily activities, a simulation was conducted with a load of 950 N to obtain the maximum deformation, maximum stress, and minimum safety factor. Direct optimization was used to simulate the dimensions (height and diameter) of the lumbar disc prosthesis model that would satisfy the safety factor, allowable load, stress, deformation, and geometry design criteria.

3.1. Distribution of stress and deformation

Simulation was performed with an applied load of 216 N. The resulting deformation of the lumbar disc prosthesis model is presented in Fig. 6, with the

maximum deformation measured at 94.27 μm. This highest deformation was detected at the posterior region of the model, which was exposed to a higher magnitude of applied load, specifically when the upper endplates were tilted. Besides, the deformation of the model showed a decrease trend upon approaching to the center of the geometry. It is envisaged that the load was distributed due to the support from the ball and socket design from the model. A similar observation was also reported in a previous study [37], where maximum deformation occurred in the posterior region of the model. On the other hand, the stress distribution of the model is depicted in Fig. 7, where the maximum stress was recorded to be 14.6 MPa. The peak stress was located at the edge of the socket (lower endplate), as evidenced by the side and top views of the lumbar disc prosthesis model.

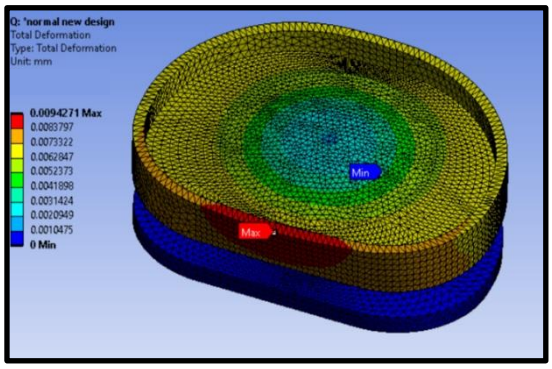

Fig. 6. Deformation of lumbar disc prosthesis model at various locations.

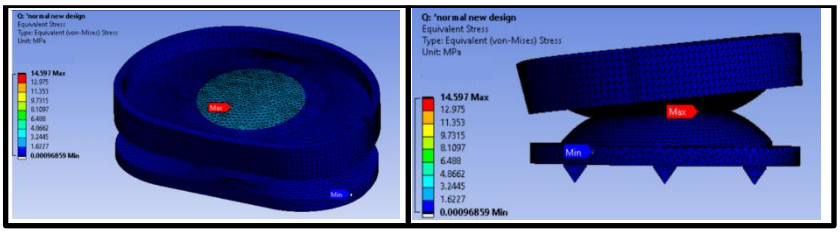

(a) Isometric view. **(b) Side view.**

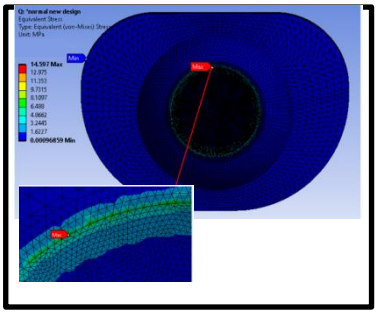

(c) Top view.

Fig. 7. Stress distribution of lumbar disc prosthesis model (a) Isometric view, (b) Side view and (c) Top view.

3.2. Flexion and extension motion

For the current design, the flexion motion of the model was recorded from neutral (90°) to 70°, which is 20° as shown in Fig. 8(a) and (b). On the other hand, the extension motion of the model was recorded from neutral to 101°, which is 11° as in Fig. 8(a) and (c). A summary of flexion and extension motion from various model in literature at L4-L5 is shown in Table 2. As compared to these findings, current design has a higher range of flexion and extension motion.

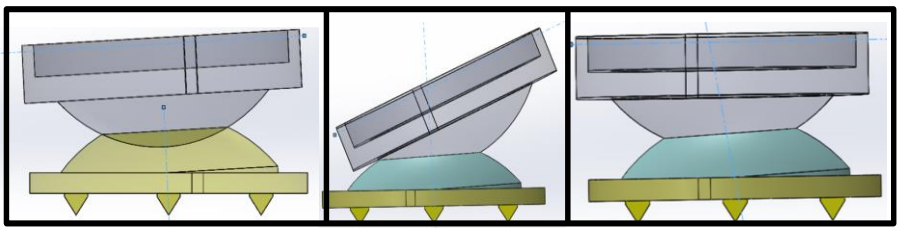

(a) Neutral Position. **(b) Flexion.** **(c) Extension.**

Fig. 8. ROM of lumbar disc prosthesis model (a) Neutral position, (b) Flexion and (c) Extension.

Table 2. Summary of flexion and extension at L4-L5 for lumbar disc prosthesis model.

Design Name	Flexion and extension (°)
Current design	20 to -11
Typical [23]	13 to -3
Charite [24]	9.6
ProDisc-L [1]	4.1 to -7.6
Maverick [38]	16.3

Figures 9 and 10 present the original and deformed lumbar disc prosthesis model, respectively, during flexion and extension at various angles. The highest deformation recorded during flexion and extension was 20.6 μm and 14.02 μm, respectively. The maximum deformation during flexion occurred at the anterior region of the model, where it experienced a higher load as compared to the posterior region. Conversely, the maximum deformation is concentrated at the posterior region during extension. The location of the deformation during flexion and extension aligns with the findings of a previous study [39], which employed titanium alloy as the implant biomaterial.

Figure 11 illustrates the location and stress distribution of the lumbar disc prosthesis model during flexion and extension. The maximum stress recorded during flexion and extension was 17.75 MPa and 14.26 MPa, respectively. The peak stress was situated at the bottom part of the lower endplate socket edge during flexion. Conversely, the maximum stress was detected at the top part of the lower endplate socket edge during extension.

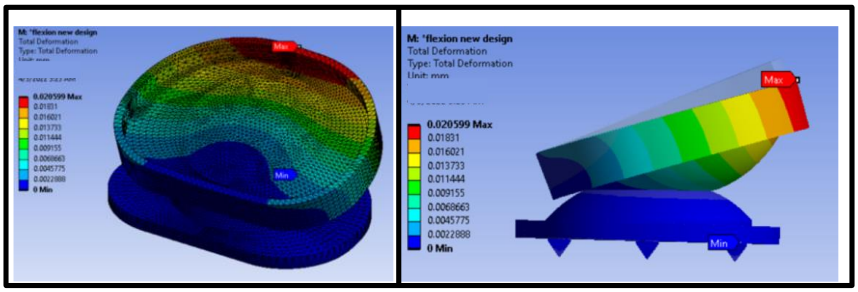

(a) Isometric view. **(b) Side view.**

Fig. 9. Deformation of the model during flexion motion (a) Isometric view and (b) Side view.

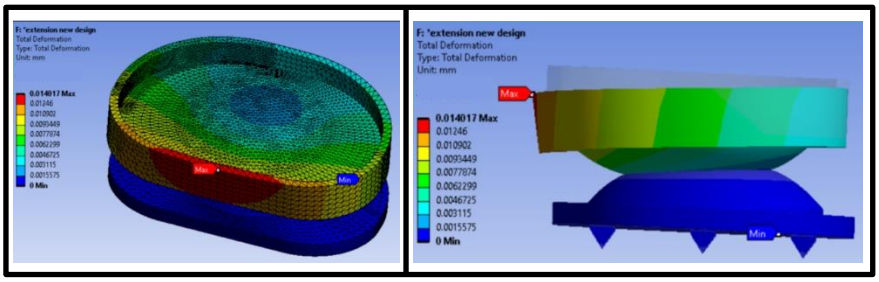

(a) Isometric view. **(b) Side view.**

Fig. 10. Deformation of the model during extension motion.

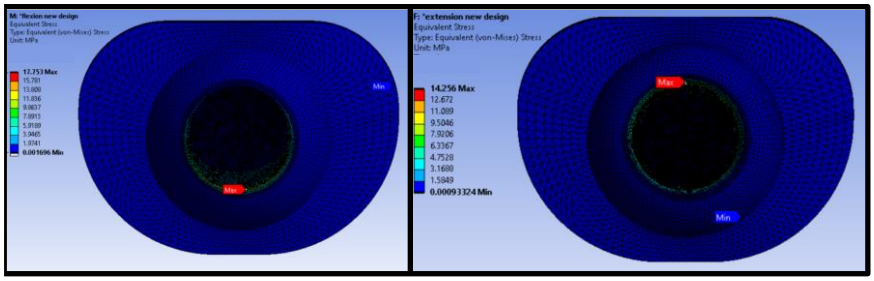

(a) Flexion. **(b) Extension.**

Fig. 11. Stress distribution of the model during flexion and extension.

3.3. Direct Optimisation

The amount of load that occurs in daily typical activity range between 200 to 950 N on the lumbar disc [40]. Simulation was conducted with a load of 950 N to obtain the maximum deformation, maximum stress and minimum safety factor. At a safety factor of 1.61, the maximum allowable stress and deformation were 70.2 MPa and 62.11 μm, respectively. Direct optimisation was used to simulate the dimension of lumbar disc prosthesis model that would satisfy the safety factor, allowable load, stress, deformation and geometry design criteria. The objectives with minimum and maximum values were defined to obtain the input parameters with the boundary conditions of the lower and upper limits of diameter and height.

For the study, 30 different variations were selected according to the limitation of the geometry design model. Figure 12 shows the effects of height and diameter on the safety factor of lumbar disc prosthesis model. The current study provides an overview of the acceptable dimension of the model according to the required safety factor. Figures 13 and 14 offer an overview of the acceptable range of dimensions according to stress and deformation. From the study, different sets of dimensions could be selected according to the required safety factor, stress and deformation upon specific applications.

According to the model and objectives, three different dimensions were recommended from the 30 variations as depicted in Table 3. The safety factor of the three candidates ranged from 2 to 2.11. Besides, the maximum stress and deformation were also found to fulfil the allowable stress (70.2 MPa) and deformation (62.11 μm) conditions.

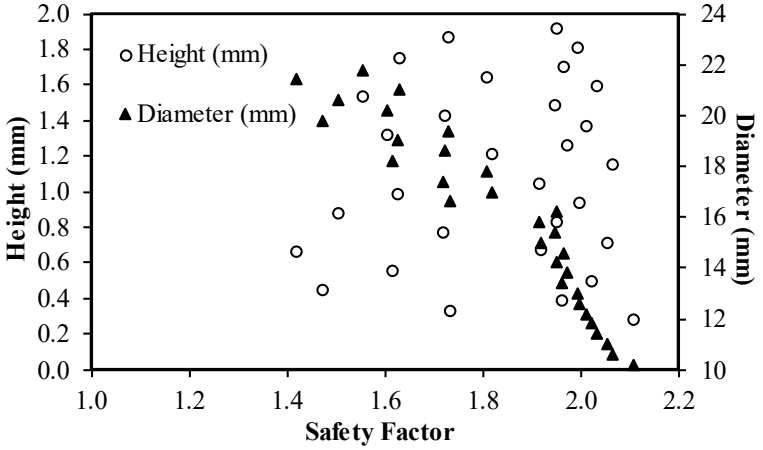

Fig. 12. The effects of height and diameter on the safety factor of lumbar disc prosthesis model.

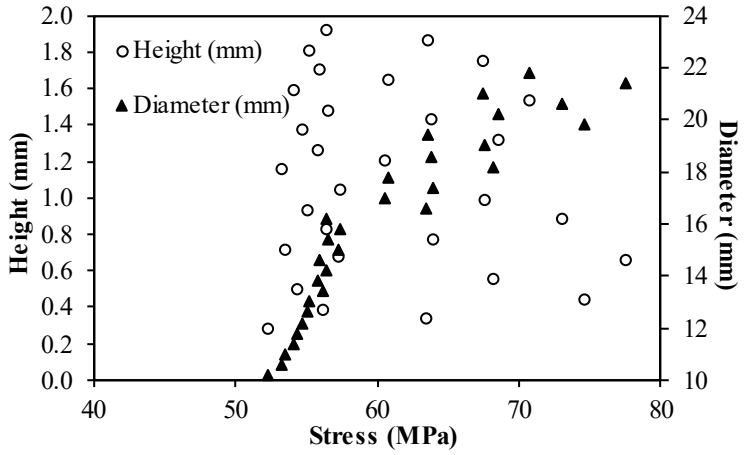

Fig. 13. The effects of height and diameter on the maximum allowable stress of lumbar disc prosthesis model.

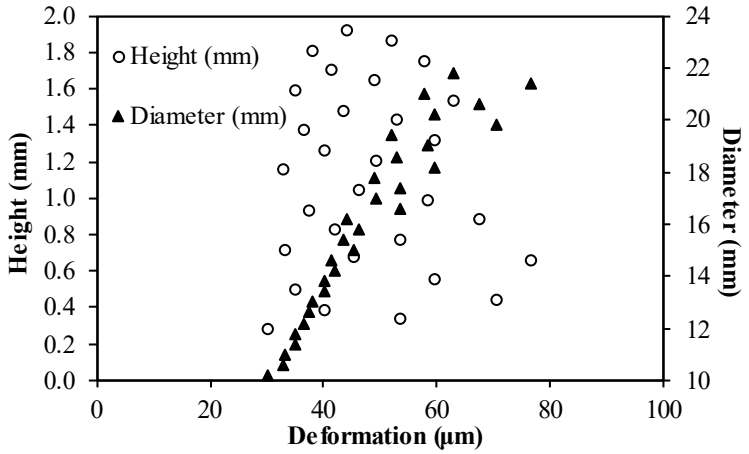

Fig. 14. The effects of height and diameter on the deformation lumbar disc prosthesis model.

Table 3. Optimised input parameters of lumbar disc prosthesis model.

Diameter (mm)	Height (mm)	Safety Factor	Stress (MPa)	Deformation (µm)
10.2	0.279	2.11	52.21	30.14
11.4	1.591	2.03	54.11	34.92
13.0	1.810	2.00	55.12	37.98

4. Conclusions

In this work, lumbar disc prosthesis at L4-L5 was successfully modelled and simulated when PEEK was used as the biomaterial. The results revealed a wide range of motion for flexion and extension from 20° to -11°. In addition, the study revealed that maximum deformation occurred at the anterior region during flexion but concentrated at the posterior region during extension. The study also offered insights into the range of acceptable dimensions for the lumbar disc prosthesis model at L4-L5, where three different sets of dimensions were proposed for reference. For future work, additional range of motion such as torsion and lateral bending could be studied. Besides, biomechanical and stresses of the lumbar disc could be investigated for non-osteoporosis and osteoporosis patients.

Abbreviations

CoCr	Chromium Alloy
DDD	Degenerative Disc Disease
FEA	Finite Element Analysis
FSU	Functional Spinal Unit
PEEK	Polyetheretherketone
PU-PC	Polyurethane Polycarbonate Elastomer
ROM	Range of Motion
Ti	Titanium
UHMWPE	Ultrahigh Molecular Weight Polyethylene

References

1. Meyers, K.N.; Campbell, D.A.; Lipman, J.D.; Zhang, K.; Myers, E.R.; Girardi, F.P.; Cammisa, F.P.; and Wright, T.M. (2007). Dynamics of an intervertebral disc prosthesis in human cadaveric spines. *HSS Journal, the Musculoskeletal Journal of Hospital for Special Surgery*, 3(2), 164-168.
2. Vanaclocha-Saiz, A.; Atienza, C.M.; Vanaclocha, V.; Belloch, V.; Santabarbara, J.M.; Jordá-Gómez, P.; and Vanaclocha, L. (2020). ICR in human cadaveric specimens: an essential parameter to consider in a new lumbar disc prosthesis design. *North American Spine Society Journal*, 2, 100016.
3. García Vacas, F.; Ezquerro Juanco, F.; Pérez de la Blanca, A.; Prado Novoa, M.; and Postigo Pozo, S. (2014). The flexion–extension response of a novel lumbar intervertebral disc prosthesis: A finite element study. *Mechanism and Machine Theory*, 73, 273-281.
4. Mathews, H.H.; Lehuec, J.C.; Friesem, T.; Zdeblick, T.; and Eisermann, L. (2004). Design rationale and biomechanics of Maverick Total Disc arthroplasty with early clinical results. *The Spine Journal*, 4(6), 268s-275s.
5. Zigler, J.E. (2004). Lumbar spine arthroplasty using the ProDisc II. *The Spine Journal*, 4(6), 260s-267s.
6. Wang, W.; Pei, B.; Wu, S.; Lu, D.; He, P.; Ma, C.; and Wu, X. (2023). Biomechanical response of four Roussouly's sagittal alignment lumbar to degeneration of different parts of intervertebral disc: finite element model analysis. *Innovation and Research in BioMedical engineering*, 44(4), 100772.
7. Goel, V.K.; Grauer, J.N.; Patel, T.C.; Biyani, A.; Sairyo, K.; Vishnubhotla, S.; Matyas, A.; Cowgill, I.; Shaw, M.; Long, R.; Dick, D.; Panjabi, M.M.; and Serhan, H. (2005). Effects of charité artificial disc on the implanted and adjacent spinal segments mechanics using a hybrid testing protocol. *Spine*, 30(24), 2755-2764.
8. Putzier, M.; Funk, J.F.; Schneider, S.V.; Gross, C., Tohtz, S.W.; Khodadadyan-Klostermann, C.; Perka, C.; and Kandziora, F. (2006). Charité total disc replacement--clinical and radiographical results after an average follow-up of 17 years. *European Spine Journal*, 15(2), 183-95.
9. Friis, E.A.; Arnold, P.M.; and Goel, V.K. (2017). Mechanical testing of cervical, thoracolumbar, and lumbar spine implants. *Mechanical Testing of Orthopaedic Implants*, Elsevier.
10. Gennari, A.; Yuh, S.; Petit, L.L.; Wang, Z.; Boubez, G.; Tarabay, B.; Shedid, D.; Gavotto, A.; Pelletier, Y.; and Litrico, S. (2022). Anterior longitudinal ligament flap technique: description of anterior longitudinal ligament opening during anterior lumbar spine surgery and review of vascular complications in 189 patients. *World Neurosurgery*, 165, e743-e749.
11. Zhang, X.-Y.; and Han, Y. (2023). Comparison of the biomechanical effects of lumbar disc degeneration on normal patients and osteoporotic patients: A finite element analysis. *Medical Engineering & Physics*, 112, 103952.
12. Li, L.; Shen, T.; and Li, Y.-K. (2017). A finite element analysis of stress distribution and disk displacement in response to lumbar rotation manipulation in the sitting and side-lying positions. *Journal of Manipulative and Physiological Therapeutics*, 40(8), 580-586.

13. Wang, W.; Zhang, H.; Sadeghipour, K.; and Baran, G. (2013). Effect of posterolateral disc replacement on kinematics and stress distribution in the lumbar spine: A finite element study. *Medical Engineering & Physics*, 35(3), 357-364.
14. Kiyani, S.; Taheri-Behrooz, F.; and Asadi, A. (2021). Analytical and finite element analysis of shape memory polymer for use in lumbar total disc replacement. *Journal of the Mechanical Behavior of Biomedical Materials*, 122, 104689.
15. Guldeniz, O.; Yesil, O.B.; and Okyar, F. (2022). Yeditepe spine mesh: Finite element modeling and validation of a parametric CAD model of lumbar spine. *Medical Engineering & Physics*, 110, 103911.
16. Raheem, H.M.; and Aljanabi, M. (2020). Studying the bulging of a lumbar intervertebral disc: A Finite Element Analysis. *Procedia Structural Integrity*, 28, 1727-1732.
17. Yee, S.L.K.; and Joon, K.T. (2021). A preliminary study on the design of compliant surgical gripper jaw. *11th International Conference on Biomedical Engineering and Technology*. Tokyo, Japan, 121-126.
18. Jie, G.L.; and Yee, S.L.K. (2019). Stress and strain analysis on knee joint. *Proceedings of the 2019 9th International Conference on Biomedical Engineering and Technology*. Tokyo, Japan, 47-50.
19. Cook, D.J.; Yeager, M.S.; and Cheng, B.C. (2015). Range of motion of the intact lumbar segment: a multivariate study of 42 lumbar spines. *International Journal of Spine Surgery*, 9(5), 1-8.
20. Roch, P.J.; Wagner, M.; Weiland, J.; Gezzi, R.; Spiering, S.; Lehmann, W.; Saul, D.; Weiser, L.; Viezens, L.; and Wachowski, M.M. (2020). Total disc arthroplasties change the kinematics of functional spinal units during lateral bending. *Clinical Biomechanics*, 73, 130-139.
21. Filardi, V.; Simona, P.; Cacciola, G.; Bertino, S.; Soliera, L.; Barbanera, A.; Pisani, A.; Milardi, D.; and Alessia, B. (2017). Finite element analysis of sagittal balance in different morphotype: Forces and resulting strain in pelvis and spine. *Journal of Orthopaedics*, 14(2), 268-275.
22. Serratrice, N.; Gennari, A.; Yuh, S.-J.; Sabah, Y.; Gavotto, A.; Paquis, P.; and Litrico, S. (2021). Segmental lordosis gain is a prognostic radiological factor of good functional outcome after the implantation of a single-level prosthesis or a hybrid construct for lumbar disc degeneration. *World Neurosurgery*, 152, e597-e602.
23. Gamradt, S.C.; and Wang, J.C. (2005). Lumbar disc arthroplasty. *The Spine Journal*, 5(1), 95-103.
24. Lemaire, J.P.; Skalli, W.; Lavaste, F.; Templier, A.; Mendes, F.; Diop, A.; Sauty, V.; and Laloux, E. (1997). Intervertebral disc prosthesis: results and prospects for the year 2000. *Clinical Orthopaedics and Related Research*, (337), 64-76.
25. Himarosa, R.A.; and Suyitno, S. (2018). Design, fabrication, and testing of prototype of total lumbar disc replacement. *Journal of Energy, Mechanical, Material, and Manufacturing Engineering*, 3(1), 1-6.
26. Du, C.F.; Cai, X.Y.; Gui, W.; Sun, M.S.; Liu, Z.X.; Liu, C.J.; Zhang, C.Q., and Huang, Y.P. (2021). Does oblique lumbar interbody fusion promote adjacent degeneration in degenerative disc disease: A finite element analysis. *Computers in Biology and Medicine*, 128, 104122.

27. Afshar-Mohajer, M.; Yaghoubi, A.; Ramesh, S.; Bushroa, A.R.; Chin, K.M.C.; Tin, C.C.; and Chiu, W.S. (2014). Electrophoretic deposition of magnesium silicates on titanium implants: Ion migration and silicide interfaces. *Applied Surface Science*, 307, 1-6.
28. Bowen, C.; Ramesh, S.; Gill, C.; and Lawson, S. (1998). Impedance spectroscopy studies of CuO-doped Y-TZP ceramics. *Journal of Materials Science*, 33, 5103-5110.
29. Mehboob, H.; Tarlochan, F.; Mehboob, A.; Chang, S.-H.; Ramesh, S.; Harun, W.S.W.; and Kadirgama, K. (2020). A novel design, analysis and 3D printing of Ti-6Al-4V alloy bio-inspired porous femoral stem. *Journal of Materials Science: Materials in Medicine*, 31, 1-14.
30. Reeks, J.; and Liang, H. (2015). Materials and their failure mechanisms in total disc replacement. *Lubricants*, 3(2), 346-364.
31. Veruva, S.Y.; Steinbeck, M.J.; Toth, J.; Alexander, D.D.; and Kurtz, S.M. (2014). Which design and biomaterial factors affect clinical wear performance of total disc replacements? A systematic review. *Clinical Orthopaedics and Related Research*, 472(12), 3759-3769.
32. Gornet, M.F.; Burkus, J.K.; Harper, M.L.; Chan, F.W.; Skipor, A.K.; and Jacobs, J.J. (2013). Prospective study on serum metal levels in patients with metal-on-metal lumbar disc arthroplasty. *European Spine Journal*, 22(4), 741-746.
33. Yin, W.; Chen, M.; Bai, J.; Xu, Y.; Wang, M.; Geng, D.; and Pan, G. (2022). Recent advances in orthopedic polyetheretherketone biomaterials: Material fabrication and biofunction establishment. *Smart Materials in Medicine*, 3, 20-36.
34. Han, X.; Yang, D.; Yang, C.; Spintzyk, S.; Scheideler, L.; Li, P.; Li, D.; Geis-Gerstorfer, J.; and Rupp, F. (2019). Carbon fiber reinforced PEEK composites based on 3D-printing technology for orthopedic and dental applications. *Journal of Clinical Medicine*, 8(2), 1-17.
35. Culemann, S.; Grüneboom, A.; and Krönke, G. (2019). Origin and function of synovial macrophage subsets during inflammatory joint disease. *Advances in Immunology*, 143, 75-98.
36. Atta-alla, E.S.; Saab, I.; Shishtawy, M.; and Haidar Hassan, K. (2014). Morphometric study of the lumbosacral spine and some of its related angles in Lebanese adult females. *Italian Journal of Anatomy and Embryology*, 119, 92-105.
37. Byrne, R.M.; Aiyangar, A.K.; and Zhang, X. (2019). A dynamic radiographic imaging study of lumbar intervertebral disc morphometry and deformation in vivo. *Scientific Reports*, 9(1), 1-12.
38. Hitchon, P.W.; Eichholz, K.; Barry, C.; Rubenbauer, P.; Ingalhalikar, A.; Nakamura, S.; Follett, K.; Lim, T.H.; and Torner, J. (2005). Biomechanical studies of an artificial disc implant in the human cadaveric spine. *Journal of Neurosurgery: Spine*, 2(3), 339-343.
39. Song, C.-H.; Park, J.-S.; Choi, B.-W.; Lee, J.S.; and Lee, C.-S. (2021). Computational investigation for biomechanical characteristics of lumbar spine with various porous Ti–6Al–4V implant systems. *Applied Sciences*, 11(17), 1-18.
40. Himarosa, R.; and Suyitno, D. (2018). Design, fabrication, and testing of prototype of total lumbar disc replacement. *Journal of Energy, Mechanical, Material and Manufacturing Engineering*, 3(1), 1-6.